



# Synthesis of Pore-Size-Tunable Mesoporous Silica Nanoparticles by Simultaneous Sol-Gel and Radical Polymerization to Enhance Silibinin Dissolution

Mina Shafiee<sup>1</sup>, PharmD;  Samirasadat Abolmaali<sup>2</sup>, PharmD, PhD;  Mozghan Abedanzadeh<sup>2</sup>, PharmD; Mehdi Abedi<sup>2</sup>, MSc; Alimohammad Tamaddon<sup>2</sup>, PharmD, PhD

<sup>1</sup>Department of Pharmaceutical Nanotechnology, School of Pharmacy, Shiraz University of Medical Sciences, Shiraz, Iran;

<sup>2</sup>Center for Nanotechnology in Drug Delivery, School of Pharmacy, Shiraz University of Medical Sciences, Shiraz, Iran

## Correspondence:

Samirasadat Abolmaali, PharmD, PhD; Department of Pharmaceutical, Nanotechnology and Research Center for Nanotechnology in Drug Delivery, Rohn Abad, Karafarin St., Postal code: 7146864685, Shiraz, Iran  
Tel: +98 9375504436

Email: [abolmaali@sums.ac.ir](mailto:abolmaali@sums.ac.ir)  
[s.abolmaali@gmail.com](mailto:s.abolmaali@gmail.com)

Received: 25 April 2020

Revised: 18 August 2020

Accepted: 07 September 2020

## What's Known

- Silibinin, a major phytochemical of milk thistle seeds indicated in chronic liver disease and cirrhosis, exhibits low solubility and, consequently, low oral bioavailability.
- Mesoporous silica nanoparticles (MSNs) are intended for drug delivery due to their small pore size (2–50 nm), high specific surface area, excellent biodegradability, and biocompatibility.

## What's New

- Synthesis of MSNs with tunable sizes and pore diameters was attained by simultaneous sol-gel reaction and free-radical polymerization.
- High capacity loading of silibinin in MSNs enhanced its dissolution and the preservation of its antioxidant activity in acidic gastric juice.

## Abstract

**Background:** Silibinin (SBN), a major active constituent of milk thistle seeds, exhibits numerous pharmacological activities. However, its oral bioavailability is low due to poor water solubility. This study aimed to develop a new synthetic approach for tuning the pore characteristics of mesoporous silica nanoparticles (MSNs) intended for the oral delivery of SBN. In addition, the effects of the pore diameter of MSNs on the loading capacity and the release profile of SBN were investigated.

**Methods:** The present study was performed at Shiraz University of Medical Sciences, Shiraz, Iran, in 2019. This synthesis method shares the features of the simultaneous free-radical polymerization of methyl methacrylate and the sol-gel reaction of the silica precursor at the n-heptane/water interface. SBN was loaded onto MSNs, the *in vitro* release was determined, and the radical scavenging activities were compared between various pH values using the analysis of variance.

**Results:** According to the Brunauer–Emmett–Teller protocol, the pore sizes were well-tuned in the range of 2 to 7 nm with a large specific surface area (600–1200 m<sup>2</sup>/g). Dynamic light scattering results showed that different volume ratios of n-heptane/water resulted in different sizes, ranging from 25 to 100 nm. Interestingly, high SBN loading (13% w/w) and the sustained release of the total drug over 12 hours were achieved in the phosphate buffer (pH=6.8). Moreover, the antioxidant activity of SBN was well preserved in acidic gastric pH.

**Conclusion:** Well-tuned pores of MSNs provided a proper substrate, and thus, enhanced SBN loading and oral dissolution and preserved its antioxidant activity. Nevertheless, further *in vitro* and *in vivo* investigations are needed.

Please cite this article as: Shafiee M, Abolmaali S, Abedanzadeh M, Abedi M, Tamaddon AM. Synthesis of Pore-Size-Tunable Mesoporous Silica Nanoparticles by Simultaneous Sol-Gel and Radical Polymerization to Enhance Silibinin Dissolution. *Iran J Med Sci*. 2021;46(6):475-486. doi:10.30476/ijms.2020.86173.1595.

**Keywords** • Nanoparticles • Silicon dioxide • Polymerization • Silibinin • Antioxidants

## Introduction

Among the compounds developed in the pharmaceutical industry, about 40% show low solubility or are completely insoluble. To improve the solubility and dissolution profile of such active agents, formulation scientists need to overcome several obstacles in

different phases of formulation development.<sup>1</sup>

Over the past decades, a plethora of different organic and inorganic nanoparticles were developed for drug delivery applications.<sup>2</sup> These materials have a great scope in the field of medicine, since they can show better pharmacokinetic and pharmacodynamic profiles. Nowadays, drug delivery based on inorganic nanomaterials such as gold nanoparticles, iron oxide nanoparticles, quantum dots, and mesoporous silica nanoparticles (MSNs) is the focal point of great scrutiny.<sup>3-5</sup> Since the discovery of M41S in the early 1990s, MSNs with pore sizes ranging from 2 to 50 nm have attracted much attention, due to their unique properties such as high surface areas and pore volumes, uniform and tunable pore sizes, excellent biodegradability and biocompatibility, and easily modifiable surface properties.<sup>6</sup> Moreover, great progress has been made in the multi-functionalization design and structure control of MSNs for their potential applications such as catalysis, adsorption, separation, sensing, and drug delivery.<sup>7,8</sup> In recent years, MSNs have served as an emerging drug delivery system for various therapeutic agents.<sup>9</sup> Silica is classified as "Generally Recognized as Safe" (GRAS), by the United States Food and Drug Administration (FDA), and is widely used in cosmetic, food, and pharmaceutical industries as rheology modifiers, suspending agents, and glidants. In addition, clinical trials are still performed with targeted silica nanoparticles for an image-guided operative sentinel lymph node mapping. In contrast to solid silica nanoparticles, a mesoporous structure allows a high drug-loading capacity and a time-dependent drug release.<sup>3,4</sup> Internal silica nanochannels with large pore volumes can provide a high surface area for drug adsorption and loading, while silanol-enriched external surfaces are easily-modified and enable sustained, controlled, targeted, and stimuli-responsive drug delivery to improve therapeutic drug efficacy.<sup>10</sup> Shen and colleagues reported that the tunable pore size of MSNs could effectively control the loading and release kinetics of ibuprofen as a poorly water-soluble drug.<sup>11</sup>

MSN synthesis follows a self-assembly mechanism, whereby the physical, chemical, and structural properties of the nanoparticle are controlled by reactant ratios and experimental conditions. Recent innovations in the synthesis of MSNs with controlled particle size, morphology, and porosity, along with their chemical stability, have made silica an attractive biomaterial for drug delivery.<sup>3, 12, 13</sup> Most often in the synthesis of MSNs, surfactants such as cationic cetyltrimethylammonium bromide

(CTAB) are employed owing to their strong association with silica precursors, which results in MSNs with small pore sizes (about 3 nm). On the other hand, many new applications of MSNs require uniform and large pore sizes in the range of 4 to 8 nm.<sup>3</sup>

Silibinin (SBN) is one of the structural isomers of the flavonoid silymarin, which is extracted from the milk thistle.<sup>14</sup> Over the past two decades, SBN has received much attention due to its anticancer and chemopreventive actions, as well as its cholesterol-lowering, cardioprotective, and neuroprotective applications. SBN is a diastereoisomeric mixture of two flavonolignans, namely SBN A and SBN B, at a ratio of approximately 1:1.<sup>15</sup> In contrast to the broad therapeutic actions of SBN, its bioavailability is limited due to low aqueous solubility, low permeability across intestinal epithelial cells, extensive phase II hepatic metabolism, and rapid excretion in the bile and urine.<sup>16</sup> Moreover, the poor oral bioavailability of SBN is attributed to its degradation in the gastric fluid, which leads to more than a 20% degradation rate over 2 hours.<sup>17</sup>

The low solubility and possible inactivation of SBN in the gastrointestinal tract can impede the oral bioavailability of SBN, requiring drug incorporation into an efficient delivery system. Therefore, various approaches have been proposed, including drug encapsulation into liposomes, polymeric micelles, nanoparticles, prodrugs, and microspheres.<sup>16</sup> It is assumed that MSNs with uniform and large pore sizes can provide a new platform for delivering poorly water-soluble phytochemicals such as SBN. For example, Cao and colleagues formulated a poorly water-soluble SBN based on polymeric porous silica nanoparticles,<sup>18</sup> and Ahmadi Nasab and others prepared MSNs for the delivery of curcumin (a poorly water-soluble phytochemical).<sup>19</sup> In light of the aforementioned research, we sought to develop well-tuned MSNs for SBN loading in high capacity with an enhanced drug dissolution rate. Unlike the conventional sol-gel method, the present MSN synthesis involves a combination of the hydrolytic condensation of tetraethyl orthosilicate (TEOS) to form silica and the simultaneous free-radical polymerization of methyl methacrylate (MMA) in a system of n-heptane/water dispersion. To optimize the delivery system, we studied the effects of the MSN pore size on the loading capacity and release profile of SBN. We also examined the impact of MSN encapsulation on preserving the antioxidant activity of SBN via the 2, 2-diphenyl-1-picrylhydrazyl (DPPH) radical scavenging assay.

## Materials and Methods

The present study was performed at Shiraz University of Medical Sciences, Shiraz, Iran, in 2019. All the applied protocols were approved by the Research Ethics Committee of Shiraz University of Medical Sciences (Code: IRSUMS.REC.1397.1129).

### Materials

TEOS ( $\geq 99\%$ ) (Merck, Germany), CTAB (Dae-Jung, South Korea), MMA, L-lysine (97%), 4,4'-Azobis (4-cyanovaleric acid) (ACVA), SBN (Sigma-Aldrich, U.S.A.), and n-heptane (Caledon, Canada) were used in the current investigation. Deionized water was produced using the MilliQ3 Integral 3 Water Purification System (Millipore, U.S.A.). All the chemicals were used as received.

### Synthesis of Mesoporous Silica Nanoparticles

The synthesis method shares the features of the simultaneous free-radical polymerization of methacrylate ester and the sol-gel reaction of the silica precursor at the n-heptane/water interface (figure 1A). The process uses a basic amino acid as the catalyst, n-heptane as the organic phase component, ACVA as the initiator, and CTAB as the cationic surfactant. Briefly, 300 mg of CTAB was dissolved in 96 mL of deionized water. The mixture was purged with nitrogen gas for 45 minutes, at 70 °C. After a clear solution was obtained, different amounts of n-heptane (6 and 45 mL) were added to the solution. After 15 minutes, respective amounts of 0.5 and 20 mg/mL of MMA, 66 mg of L-lysine, 3000 mg of TEOS, and 0.81 mg/mL of ACVA were added to the reaction mixture, while it was stirred at 750 rpm (table 1). After four hours, the resulting

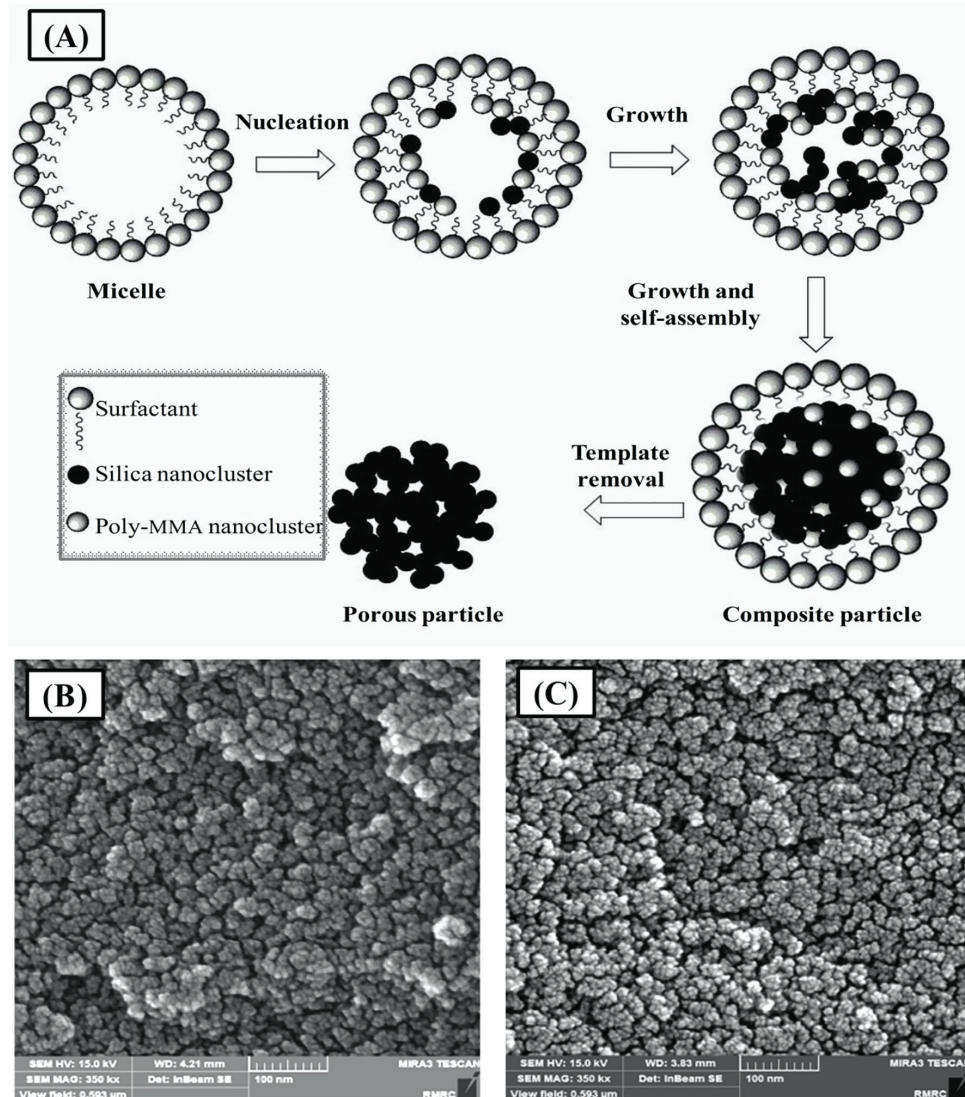


**Figure 1:** Schematic synthesis route is presented for the preparation of hybrid nanoparticles, composed of mesoporous silica and poly MMA. (A) FE-SEM micrographs correspond to the H1M1 (B) and H2M2 (C) preparations. MMA: Methyl methacrylate; FE-SEM: Field emission scanning electron microscopy; H1M1: A formulation prepared with 6 mL of n-heptane and 0.5 mg/mL of MMA; H2M2: A formulation prepared with 45 mL of n-heptane and 20 mg/mL of MMA



**Table 1:** Different MSN formulations, as well as Brunauer–Emmett–Teller and Dynamic light scattering results

Sample	Reagent Variation	Mean Particle Size (nm)	Pore Size (nm)	Surface Area (m <sup>2</sup> g <sup>-1</sup> )	Pore Volume (cm <sup>3</sup> g <sup>-1</sup> )	Silibinin Loading Capacity (%)
H0M0 (Control)	Without adding n-heptane and MMA	106.0	2.40	1193.00	1.44	0.99
H1M1	6 mL of n-heptane and 0.5 mg/mL of MMA	44.6	5.60	747.56	0.96	9.6
H2M2	45 mL of n-heptane and 20 mg/mL of MMA	25.9	7.10	606.68	1.10	13.0

MSN: Mesoporous silica nanoparticles; BET: Brunauer–Emmett–Teller; DLS: Dynamic light scattering; MMA: Methyl methacrylate; H0M0: A formulation prepared without adding n-heptane and MMA; H1M1: A formulation prepared with 6 mL of n-heptane and 0.5 mg/mL of MMA; H2M2: A formulation prepared with 45 mL of n-heptane and 20 mg/mL of MMA

product showed homogeneous milky colloidal dispersion. It was then cooled down to room temperature and decanted. The organic template and surfactant were removed by heating the raw products in an oven (500 °C) for five hours. The final product was kept in a desiccator until use. MSN products were characterized using field emission scanning electron microscopy (FE-SEM), the Brunauer–Emmett–Teller (BET) protocol, X-ray diffraction (XRD), and dynamic light scattering (DLS).

#### Characterization of Mesoporous Silica Nanoparticles

##### Field Emission Scanning Electron Microscopy

The morphology and particle size of the gold-coated samples were characterized using FE-SEM (TESCAN, U.S.A.) operated at 15 kV.

##### Nitrogen Adsorption

The pore characteristics of the samples were studied by determining nitrogen adsorption isotherms using a surface area and pore size analyzer (Micrometrics, U.S.A.) at -196 °C through the BET protocol. Before the commencement of the experiment, the powder samples (≤200 mg) were transferred to a bulb and evacuated to a pressure of 10<sup>-4</sup> Pa at 50 °C for 24 hours. The specific surface area was estimated from the nitrogen adsorption data over a relative pressure (P/P<sub>0</sub>), ranging from 0.0 to 1.0. Pore size distributions and pore volumes were also calculated using the Barrett–Joyner–Halenda protocol.<sup>20</sup>

##### X-Ray Diffraction

The XRD patterns of the samples were collected using an X-ray diffractometer (Thermo ARL, England) equipped with a CuKα target as a source for radiation at 30 kV and 30 mA. Data were obtained from small (0.7° to 10°) and wide (2° to 50°) diffraction angles (2θ) with a

step size of 0.02° and a scanning speed of 4°/min radiation. The average crystallite size was calculated from the XRD data using the Debye–Scherrer equation, as follows:<sup>21</sup>

$$\tau = \frac{0.9\lambda}{\beta \cos\theta}$$

where τ is the crystallite size, λ is the X-ray wavelength (1.54 [Å]), β is the full width at half maximum, and θ is the scattering angle of the (100) diffraction peak.

##### Dynamic Light Scattering

The particle size distribution of the MSNs in deionized water was determined using an in situ particle size analyzer (Microtrac, U.S.A.) based on 180° heterodyne light scattering and a proprietary controlled reference method.

##### Silibinin Loading onto Mesoporous Silica Nanoparticles

SBN was loaded onto the MSNs via the direct addition method. Briefly, the SBN solution in absolute ethanol was added to the MSNs and slowly mixed for 24 hours at 40 °C in different SBN/MSN weight ratios (0.07, 0.134, 0.2, 0.45, 0.7, 1, 1.4, 2, and 3). Immediately after the loading process, the particles were centrifuged at 12 000 rpm for 30 minutes. The equilibrium concentration of free SBN was assayed by ultraviolet-visible (UV-Vis) spectroscopy at a maximum wavelength (λ<sub>max</sub>) of 287 nm according to the standard curve plotted for standard solutions in the range of 5 to 200 μg/mL. The loaded amount of SBN was determined directly after the MSNs were solubilized by adding 0.1 mL of hydrofluoric acid, which was thereupon diluted to 1 mL with absolute ethanol and detected via UV-Vis spectroscopy. Afterwards, the loading efficiency and the loaded SBN amount were calculated using the following equations:<sup>22</sup>

Loading efficiency (%) =

$$\frac{\text{Amount of loaded silibinin (mg)}}{\text{Amount of the silibinin loaded (mg)}} * 100$$

$$\text{Loaded amount (\%)} = \frac{\text{Amount of loaded silibinin (mg)}}{(\text{Amount of loaded silibinin (mg)} + \text{Amount of MSN (mg)})} * 100$$

### Silibinin Adsorption Isotherms

The data on drug loading were fitted to various adsorption isotherms to explain the underlying mechanism of SBN adsorption onto the MSNs. Different adsorption models were utilized, including Langmuir, Freundlich, Dubinin–Radushkevich, and Temkin.<sup>23</sup> In contrast to the Freundlich isotherm, which is used when heterogenous and multilayer adsorption occurs, the Langmuir isotherm explains homogeneous and monolayer adsorption with no interactions between the adsorbed molecules. The Dubinin–Radushkevich model is applied in multilayer adsorption phenomena with the Gaussian energy distribution onto heterogeneous surfaces. The Temkin model assumes the effects of indirect adsorbate/adsorbate interactions. The linearized forms of the model equations were drawn upon to verify the best-fitted model, as follows:<sup>23</sup>

*Langmuir Equation:*  $1/q_e = 1/C_e \times 1/(K_L \cdot q_{max}) + 1/q_{max}$

*Freundlich Equation:*  $\text{Log}(q_e) = \text{Log}(K_f) + 1/n \times \text{Log}(C_e)$

*Dubinin–Radushkevich Equation:*  $\text{Ln}(q_e) = \text{Ln}(q_{max}) - \beta \times \varepsilon^2$ ,  $\varepsilon = R \times T \times \text{Ln}(1 + 1/C_e)$

*Temkin Equation:*  $q_e = B_T \times \text{Ln}(K_T) + B_T \times \text{Ln}(C_e)$

where  $q_e$  is the amount of SBN adsorbed per unit mass of MSNs ( $\text{mg} \cdot \text{g}^{-1}$ ),  $C_e$  is the concentration of unadsorbed SBN at equilibrium ( $\text{mg} \cdot \text{l}^{-1}$ ),  $q_{max}$  is the monolayer saturation capacity ( $\text{mg} \cdot \text{g}^{-1}$ ),  $K_L$  is the Langmuir constant related to adsorption capacity ( $\text{mg} \cdot \text{g}^{-1}$ ),  $K_f$  and  $1/n$  are the respective Freundlich adsorption capacity and intensity,  $\beta$  is the Dubinin–Radushkevich constant,  $\varepsilon$  is the Polanyi potential,  $R$  is the gas constant ( $8.31 \text{ J} \cdot \text{mol}^{-1} \cdot \text{K}^{-1}$ ),  $T$  is the absolute temperature ( $^{\circ}\text{K}$ ),  $B_T$  is the Temkin constant related to adsorption energy ( $\text{J} \cdot \text{mol}^{-1}$ ), and  $K_T$  is the Temkin binding constant ( $\text{L} \cdot \text{g}^{-1}$ ).

### In Vitro Release Kinetics

The release of the loaded SBN from the formulation prepared with 6 mL of n-heptane and 0.5 mg/mL of MMA (H1M1), and the formulation prepared with 45 mL of n-heptane and 20 mg/mL of MMA (H2M2) was investigated in comparison with the equivalent amount of the free drug powder. Accordingly, an accurately weighed amount of each sample was dispersed in deionized water by

bath sonication and transferred into the dialysis tubing (cutoff=6–8 KD). The samples were transferred into the dialysis tubing (cutoff=6–8 KD) and immersed in 10 mL of a simulated gastric fluid (0.1N of the hydrochloric acid buffer solution, pH=1.2) and a simulated intestinal fluid (phosphate buffer [pH=6.8], containing 0.5% Pluronic F-127 to maintain sink condition) for 12 hours at 37 °C while shaking at 50 rpm. At predefined time intervals, an aliquot of 0.1 mL was withdrawn from the release medium and replaced by the same volume of the fresh medium. The SBN concentration in the release medium was determined by UV-Vis spectroscopy at a  $\lambda_{max}$  of 287 nm. The cumulative percentage of SBN release was plotted against time. The kinetics of the drug release was analyzed by fitting the data through different mathematical models (zero-order, first-order, Higuchi, Korsmeyer–Peppas, and Hixson–Crowell). The most appropriate model was chosen based on the R-squared ( $R^2$ ), as was similarly reported in other studies.<sup>24, 25</sup>

### 2, 2-Diphenyl-1-Picrylhydrazyl Free Radical Scavenging Activity

The free radical scavenging activity of SBN at different pH levels was determined by DPPH, a stable organic radical, which undergoes a color change from violet to yellow with H-donor antioxidants.<sup>26</sup> Accordingly, DPPH (2 mg) was dissolved in 20 mL of ethanol to make a stock solution. Thereafter, 200  $\mu\text{g}/\text{mL}$  of free SBN or an equivalent amount of the SBN-loaded MSNs was dispersed in aqueous media at pH levels of 1.2, 4.5, and 6.8. An aliquot of the samples was incubated at 37 °C for 48 hours. Subsequently, 200  $\mu\text{L}$  of 0.1 mM of the DPPH solution was added to 20  $\mu\text{L}$  of the samples withdrawn at different time intervals and incubated in a dark room for 30 min. UV absorbance intensity was measured at 517 nm, and the antioxidant activity was calculated as inhibition (%) according to the following equation:<sup>27</sup>

$$\text{Inhibition (\%)} = (1 - (A_s/A_c)) \times 100$$

where  $A_s$  and  $A_c$  are the absorbance of the sample and the control (SBN-free medium), respectively.

### Statistical Analysis

Replicate data were expressed as the mean  $\pm$  SD ( $n=3$ ). The statistical analyses were performed using the Prism software (version 5, GraphPad, USA). The physicochemical attributes of the formulations were compared using the one-way analysis of variance (ANOVA) and the Tukey *post-hoc* tests was used to evaluate the significant differences between the groups. In addition, at each pH level, changes

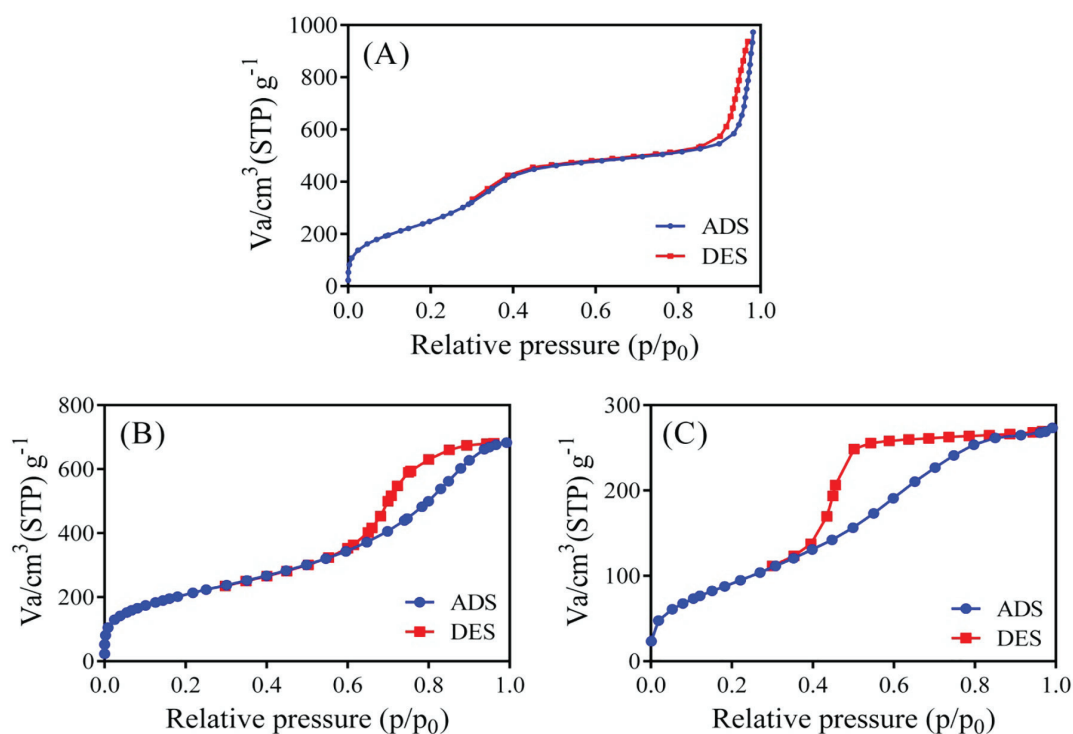


**Figure 2:**  $N_2$  adsorption/desorption isotherms of the (A) H0M0, (B) H1M1, and (C) H2M2 are presented in different relative pressures. ADS: Adsorption; DES: Desorption; MMA: Methyl methacrylate; H0M0: A formulation prepared without adding n-heptane and MMA; H1M1: A formulation prepared with 6 mL of n-heptane and 0.5 mg/mL of MMA; H2M2: A formulation prepared with 45 mL of n-heptane and 20 mg/mL of MMA

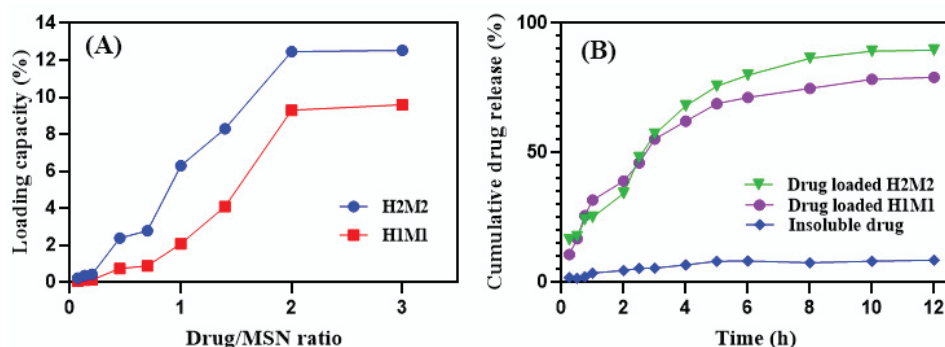


**Figure 3:** A) SBN amount (%) loaded onto the MSNs is shown as a function of the drug/MSN weight ratio. B) Cumulative drug release (%) was determined in the SBN-loaded H1M1 and H2M2 and the free SBN powder in acidic gastric juice (pH=1.2) for 2 hours and then in the phosphate buffer (pH=6.8) for 10 hours. SBN: Silibinin; MSN: Mesoporous silica nanoparticles; MMA: Methyl methacrylate; H1M1: A formulation prepared with 6 mL of n-heptane and 0.5 mg/mL of MMA; H2M2: A formulation prepared with 45 mL of n-heptane and 20 mg/mL of MMA

in the antioxidant activities of the samples (H2M2-loaded vs. free SBN) were compared between various incubation times using the repeated-measure ANOVA, while the sample was considered to be a covariate. P values of less than 0.05 were considered statistically significant.

## Results

### Morphology, Particle Size, and Pore Characterization of Mesoporous Silica Nanoparticles

MSN morphology and particle size were characterized by FE-SEM and DLS. As is shown in the FE-SEM micrographs (figures 1B

and C), the H1M1 and H2M2 samples similarly showed spherical particle morphologies with a cauliflower-like association. The DLS experiment results revealed that hydrodynamic sizes were roughly in the range of 25 to 100 nm, depending on the reaction condition (table 1).

The pore characteristics of the MSNs were determined from the  $N_2$  adsorption/desorption isotherms (figure 2). Table 1 summarizes the BET analysis results. The pore sizes ranged from 2 to 7 nm, and the specific surface areas varied from 1200 to 600  $m^2/g$ .

### Silibinin Loading

Figure 3A depicts the drug loading of the

H1M1 and the H2M2, indicating the higher loading of SBN onto the H2M2 in various weight ratios. In contrast to the control sample (H0M0), which showed only the drug loading of about 1%, the loading capacity increased to about 13% for the H2M2 at the SBN/MSN ratio of 2. The mechanism of drug loading was further elucidated by employing different adsorption isotherms to fit the experimental data.  $R^2$  was used to select the best model (table 2), indicating that the Freundlich adsorption was the best-fitted model with  $R^2$  of 0.95 for SBN adsorption similarly onto the H1M1 and the H2M2.

#### X-Ray Diffraction Pattern

The XRD experiment was first performed to investigate the order of the MSN pores at  $2\theta$  in the range of  $0.7^\circ$  to  $10^\circ$  (figure 4A), which confirmed a typical XRD pattern of MCM-41 with a 2D hexagonal symmetry for the H1M1 and the H2M2.<sup>28</sup> Individual intense peaks were found similarly at  $2\theta$  around two for the H1M1 and the H2M2, which could be attributed to (100) reflection.

The possible changes in the physical state of SBN after loading onto the H2M2 were further investigated by repeating the XRD experiment, but for  $2\theta$  in the range of  $2^\circ$  to  $50^\circ$  (figure 4B). It was evident that the free SBN powder showed diffraction peaks at  $2\theta$  of  $14.48^\circ$ ,  $17.16^\circ$ ,  $19.56^\circ$ ,  $22.28^\circ$ ,  $24.48^\circ$ , and  $26.82^\circ$ . Some of the peaks

were sharp and intense, which indicated the crystalline nature of SBN. In contrast, the X-ray diffractogram of the SBN-loaded MSNs showed the complete disappearance of the characteristic crystalline peaks. The broad peak around  $22^\circ$  confirmed the existence of amorphous silica in the H2M2, as was similarly reported elsewhere.<sup>29</sup> Additionally, three small peaks at  $2\theta$  of  $2.34^\circ$ ,  $4.14^\circ$ , and  $5.36^\circ$  were observed, which were related to the characteristic (100), (110), and (200) reflections of the H2M2.<sup>30</sup>

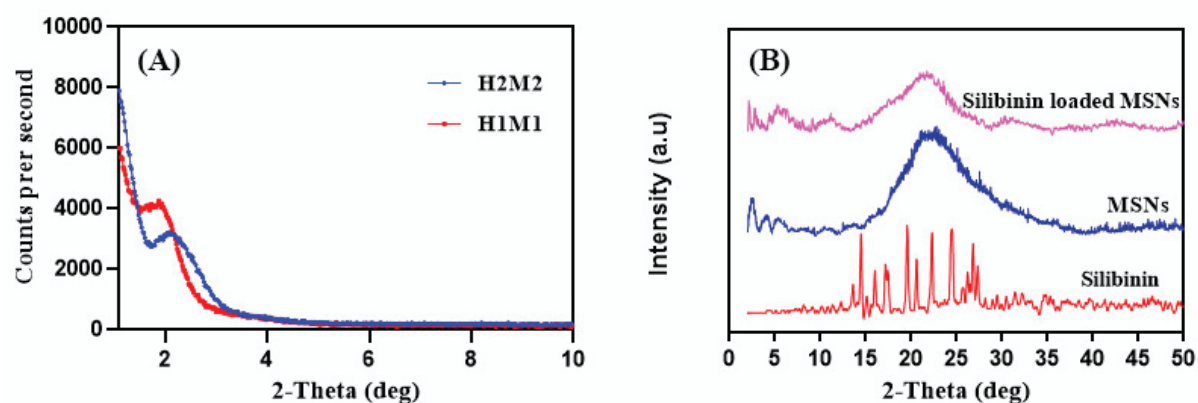
#### In Vitro Release

Figure 3B illustrates the SBN release profile of the H1M1 and the H2M2 compared with the equal quantity of the free drug powder. The results indicated that the SBN-loaded H1M1 and H2M2 comparably exhibited a typical sustained-release pattern over 12 hours and a significant ( $P < 0.001$ ) enhancement in SBN solubility compared with the free SBN powder. On the other hand, a more sustained drug release at early times, followed by a faster release, were noticed in the H2M2 formulation compared with the H1M1 formulation. The SBN release profiles were compared through the calculation of the mean dissolution time (MDT), the dissolution efficiency percentage (DE%), and the similarity factor (F2) (table 3). The F2 value was less than 50, and the MDT and DE% factors were found to be higher in the H2M2 than the H1M1.

**Table 2:** Adsorption isotherm parameters and correlation coefficients ( $R^2$ ) for the H1M1 and the H2M2

Sample	Langmuir			Freundlich			Temkin			Dubinin–Radushkevich		
	$Q_m$ (mg/g)	$K_L$ (L/g)	$R^2$	$K_F$ (L/g)	$n$	$R^2$	$K_T$ (L/g)	$B_T$ (J/mol)	$R^2$	$Q_s$ (mg/g)	$K_D$ ( $\text{mol}^2/\text{kJ}^2$ )	$R^2$
H1M1	78.7	$2.6 \times 10^{-5}$	0.93	$3 \times 10^{-4}$	0.77	0.95	$1.3 \times 10^{-3}$	9.08	0.78	11.0	0.18	0.75
H2M2	286.4	$2.3 \times 10^{-5}$	0.93	$1 \times 10^{-3}$	0.76	0.95	$1.3 \times 10^{-3}$	28.5	0.81	35.1	0.18	0.76

MMA: Methyl methacrylate; H1M1: A formulation prepared with 6 mL of n-heptane and 0.5 mg/mL of MMA; H2M2: A formulation prepared with 45 mL of n-heptane and 20 mg/mL of MMA;  $R^2$ : Correlation coefficients;  $Q_m$ : Monolayer saturation capacity;  $K_L$ : Langmuir constant;  $K_F$ : Freundlich adsorption capacity;  $n$ : Freundlich exponent;  $K_T$ : Temkin binding constant;  $B_T$ : Temkin constant related to adsorption energy;  $Q_s$ : Theoretical isotherm saturation capacity;  $K_D$ : Dubinin–Radushkevich isotherm constant



**Figure 4:** Low-angle X-ray diffractograms were overlaid for the unloaded H1M1 and H2M2, and (A) wide-angle X-ray diffractograms were compared between the SBN-loaded H2M2, free SBN powder, and unloaded H2M2 samples (B). SBN: Silibinin; MSN: Mesoporous silica nanoparticles; MMA: Methyl methacrylate; H1M1: A formulation prepared with 6 mL of n-heptane and 0.5 mg/mL of MMA; H2M2: A formulation prepared with 45 mL of n-heptane and 20 mg/mL of MMA



**Table 3:** Independent model parameters for the release of silibinin from the H1M1 and the H2M2

Sample	MDT (h)	DE%	F2
H1M1	2.87	64.8	21.6
H2M2	3.15	71.8	

MDT: Mean dissolution time; DE%: Dissolution efficiency percentage; MMA: Methyl methacrylate; H1M1: A formulation prepared with 6 mL of n-heptane and 0.5 mg/mL of MMA; H2M2: A formulation prepared with 45 mL of n-heptane and 20 mg/mL of MMA; F2: Similarity factor (an index calculated for the H1M1 in comparison with the H2M2 or vice versa)

**Table 4:** Kinetic parameters for silibinin release from the H1M1 and the H2M2

Sample	Zero-Order		First-Order		Higuchi		Korsmeyer–Peppas		Hixson–Crowell	
	$K_0$	$R^2$	$K_1$	$R^2$	$K_H$	$R^2$	N	$R^2$	$K_{HC}$	$R^2$
H1M1	14.48	0.95	0.49	0.83	33.6	0.98	0.57	0.96	0.29	0.96
H2M2	14.33	0.96	0.44	0.97	38.3	0.95	0.62	0.96	0.30	0.95

MMA: Methyl methacrylate; H1M1: A formulation prepared with 6 mL of n-heptane and 0.5 mg/mL of MMA; H2M2: A formulation prepared with 45 mL of n-heptane and 20 mg/mL of MMA;  $R^2$ : Correlation coefficients;  $K_0$ : Zero-order release constant;  $K_1$ : First-order rate constant;  $K_H$ : Higuchi dissolution constant; N: Release exponent;  $K_{HC}$ : Hixson–Crowell rate constant

The mechanism of SBN release was investigated by fitting the release data in zero-order, first-order, Higuchi, Korsmeyer–Peppas, and Hixson–Crowell mathematical models. As is presented in table 4, the Higuchi model was best fitted according to the model's  $R^2$ .

## 2, 2-Diphenyl-1-Picrylhydrazyl Free Radical Scavenging

The DPPH free radical scavenging assay was applied to determine the antioxidant activity of SBN at different pH levels. In contrast to the medium pH levels of 4.5 and 6.8, which did not cause any significant change in DPPH inhibition (%) ( $P=0.2$ ), the antioxidant activity of free SBN decreased after exposure to acidic gastric juice (pH=1.2). Interestingly, the SBN-loaded H2M2 showed more antioxidant activity than free SBN at a pH of 1.2 (figure 5).

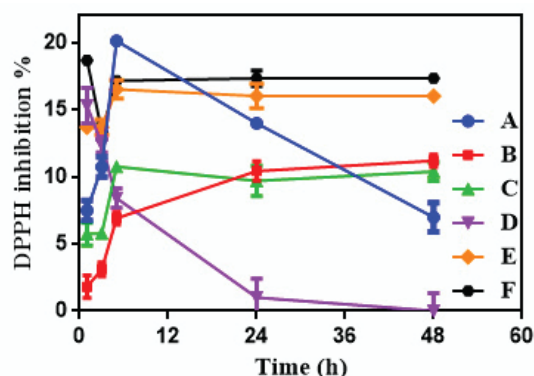


**Figure 5:** The figure shows the DPPH inhibition (%) of the silibinin-loaded H2M2 at a pH of 1.2 (A), pH of 4.5 (B), and pH of 6.8 (C), and free silibinin at a pH of 1.2 (D), pH of 4.5 (E), and pH of 6.8 (F) after incubation at 37 °C. DPPH: 2, 2-diphenyl-1-picrylhydrazyl; MMA: Methyl methacrylate; H2M2: A formulation prepared with 45 mL of n-heptane and 20 mg/mL of MMA; Replicate data were expressed as the mean±SD (n=3). DPPH inhibitions (%) were compared at a certain pH between the silibinin-loaded H2M2 and free silibinin using the one-way analysis of variance and the Tukey post-hoc tests was used to evaluate the significant differences between the groups.

## Discussion

MSNs are routinely synthesized through the sol-gel reaction of silica precursors in the presence of soft-templating materials (e.g., CTAB).<sup>31</sup> However, such syntheses are hampered by several issues such as small pore sizes and unfavorable pore morphologies for high-capacity drug loading. In the present study, we developed a one-pot synthesis method based on the combination of the sol-gel of the TEOS precursor and the radical polymerization of the MMA monomer in n-heptane/water dispersion. Aiming to simultaneously tune the particle size and the pore diameter, we performed the reactions in different n-heptane volume ratios and MMA monomer concentrations. Interestingly, the particle sizes decreased in tandem with increases in the n-heptane volume, possibly because the n-heptane/water interface can adsorb particles and prevent their aggregation in the bulk medium, as was explained elsewhere,<sup>32</sup> and it was shown that high concentrations of MMA resulted in larger pores, as was similarly described by Zhang and colleagues.<sup>33</sup> Moreover, the specific surface area decreased in parallel with increases in MMA concentrations due to the formation of larger pores.

We determined the pore characteristics of MSNs from  $N_2$  adsorption/desorption isotherms. A hysteresis pattern indicates a porous silica structure. The International Union of Pure and Applied Chemistry (IUPAC) has classified the hysteresis pattern into four types: designated H1 to H4, which correspond to pore shapes.<sup>34</sup> Accordingly, the hysteresis pattern of the H0M0 sample mostly resembles type H1, which corresponds to cylindrical pores, whereas the hysteresis pattern of the H2M2 bears a resemblance to type H2 (ink bottle) pores. The H1M1 showed an intermediate property, indicating a shift from type H1 to H2 hysteresis pattern. The appearance of the  $H_2$  pattern can



be due to the prevention of  $N_2$  desorption from narrow-necked pores.<sup>35</sup>

We loaded SBN, a poorly water-soluble phytochemical drug, onto the MSNs in different weight ratios of SBN to MSN, as was similarly studied for curcumin.<sup>19</sup> Likewise, Cao and colleagues formulated porous silica nanoparticles via the reverse microemulsion method, which showed only 5% silymarin loading (the standardized extract of milk thistle seeds).<sup>36</sup> Fazio and colleagues prepared a system composed of poly(ethylene glycol)-poly(lactic-co-glycolic acid)-Au (PEG-PLGA-Au), which showed about 8.8% SBN loading.<sup>37</sup> The high capacity loading of SBN in the H2M2 (13%) compared with that in the mentioned studies confirms the suitability of the MSN carrier for SBN delivery.

The amount of the loaded SBN was influenced by the pore size, indicating the high loading capacity of the H2M2, with the mean pore size of 7 nm, in comparison with the control sample (H0M0), with the mean pore size of 2 nm. Although the H2M2 provided a lower specific surface area for SBN adsorption, its larger pores impeded the SBN transport into and out of the pores less; hence, we attained higher SBN loading with the H2M2. The Freundlich adsorption was the best-fitted model in SBN adsorption similarly on the H1M1 and the H2M2 particles. This model is generally used to describe heterogenous and multilayer adsorption phenomena.<sup>29</sup> Interestingly, the high  $K_f$  calculated for the H2M2 compared with the H1M1, indicated increased adsorption capacity by the MSNs with larger pore diameters. In addition,  $1/n$  values of greater than 1 were indicative of S-type isotherms, which are commonly observed for the compounds containing polar functional groups.<sup>38</sup> At low adsorbate concentrations, it appears that ethanol can compete with SBN, which results in low-affinity adsorption. However, with increasing SBN concentrations, the surface adsorption initially increases and eventually decreases until it becomes zero as vacant adsorbent sites are thoroughly filled.<sup>39</sup>

To investigate the order of the MSN pores, we performed the XRD experiment at  $2\theta$  in the range of  $0.7^\circ$  to  $10^\circ$ . The peak positions 100 at  $2\theta$  were less than  $2.5^\circ$  (corresponding to the average  $d$ -spacing=4.4 nm), indicating mesoporous materials.<sup>40</sup> In addition, the crystallite size was calculated to be 15.4 and 13.8 nm in the H1M1 and the H2M2, respectively. The reflections of 110 and 200 were not easily seen in the obtained diffractograms, which can be due to their very low intensity, which is in the same line with a previous study.<sup>41</sup> To further investigate the possible changes in the physical state of SBN after loading onto the H2M2, we carried out the

XRD experiment for  $2\theta$  in the range of  $2^\circ$  to  $50^\circ$ . Unlike the X-ray diffractogram of the free SBN powder, which showed some sharp and intense peaks of the crystalline SBN powder, as was reported by Patel and colleagues,<sup>17</sup> the SBN loaded onto the MSNs presented the complete disappearance of such peaks, suggesting the formation of amorphous SBN after loading onto the MSNs, probably due to the suppression of drug crystallization in the confined mesopores of the H2M2, as was similarly explained by Patel and others<sup>17</sup> and Sahibzada and colleagues.<sup>42</sup>

The SBN release profile showed that both SBN-loaded H1M1 and H2M2 formulations provided a typical sustained-release pattern over 12 hours and significantly enhanced drug dissolution, by comparison with the free SBN powder. Similarly, Patel and colleagues prepared shellac colloidal particles containing SBN, which showed a 90% release rate over 4 hours.<sup>17</sup> In another study, Cao and others showed a very sustained release of silymarin from porous silica nanoparticles (about 13% after 72 h).<sup>36</sup> In addition, Lu and colleagues formulated hydroxypropyl methylcellulose matrix tablets, which showed a 20% SBN release rate over 12 hours.<sup>43</sup> It seems that the enhanced SBN dissolution, as is shown in the present study, can be due to not only the conversion of the crystalline SBN powder into the microcrystalline or amorphous state via loading onto mesopores, as was demonstrated in the XRD diffractograms, but also the formation of large mesopores in the silica matrix, which enhanced the SBN transport out of the particles. Furthermore, with respect to the F2 value, which was calculated to be less than 50, we did not consider the release profiles to be similar. Importantly, we found higher MDT and DE% factors in the H2M2 than the H1M1, which can be explained by the large ink-bottle pores in the H2M2, as was explained before. As is presented before, it was difficult for us to choose the proper release kinetic model owing to the close similarity of  $R^2$  in different models. The Higuchi model fitted the release data, confirming that passive diffusion was involved in SBN release from the insoluble matrix, as was similarly explained elsewhere for MCM-41 nanoparticles.<sup>41</sup> The rate constant ( $K_H$ ) was determined to be higher for the H2M2 than the H1M1, which can be due to the larger pores of the H2M2. The underlying mechanism of SBN release was investigated through the calculation of the Korsmeyer–Peppas release exponent ( $n$ ): the calculated figure was between 0.45 to 0.89, indicating that the drug release deviated from the Fickian diffusion.<sup>44</sup> Such a deviation from the classical passive diffusion mechanism can be explained by the slow degradation of

the amorphous silica matrix over time, as was explained elsewhere.<sup>45</sup>

The sustained release of SBN from the H2M2 resulted in a more retained DPPH free radical scavenging activity of SBN in the supernatant than the free powder SBN, which was significantly apparent at a pH of 1.2. Mean differences in DPPH inhibition (%) were determined to be  $5.18\% \pm 2.13\%$ ,  $1.05\% \pm 1.84\%$ , and  $1.59\% \pm 0.74\%$  at pH levels of 1.2, 4.5, and 6.8, respectively. Similarly, Patel and colleagues reported that shellac colloidal particles attenuated SBN degradation at a pH of 1.2.<sup>17</sup> Moreover, it was reported that SBN dimers could be formed by phosphodiester bonds between -OH groups after exposure to the phosphate buffer,<sup>15</sup> which can explain the preservation of SBN activity in this medium (pH=6.8) in comparison with acidic gastric juice (pH=1.2).

## Conclusion

In the present study, a new preparation method was developed for the synthesis of MSNs to enhance the loading and dissolution of poorly water-soluble phytochemicals (e.g. SBN). This preparation method shares the features of the simultaneous free-radical polymerization of the MMA monomer and the sol-gel reaction of the silica precursor (TEOS) at the n-heptane/water interface. Pore sizes and particle diameters were drastically affected by changing the monomer concentration and the n-heptane/water volume ratio, respectively. FE-SEM micrographs showed that the MSNs had a spherical shape. The BET analysis results confirmed the control of the pore size and the specific surface area in the range of 2 to 7 nm and 600 to 1200 m<sup>2</sup>/g, respectively. The DLS data disclosed that the different volumes of n-heptane resulted in different particle sizes, ranging from 25 to 100 nm. Interestingly, SBN loading was pore-size dependent in that it changed from 9 to 13% w/w in the MSNs with the pore size of 5 and 7 nm, respectively. Our *in vitro* release study indicated that, unlike free SBN, which exhibited extremely low dissolution efficiency, the SBN-loaded MSNs offered a typical sustained-release of about 90% over 12 hours. Concurrently, better preservation of SBN in the acidic gastric pH (1.2) was attained via loading onto the H2M2. Altogether, well-tuned MSNs can confer poorly water-soluble phytochemicals such as SBN sustained release, augmented preservation, and enhanced oral bioavailability. Finally, further *in vitro* and *in vivo* investigations are needed to study other aspects of this formulation; for example, the possible toxicity of MSNs and the residual MMA monomer.

## Acknowledgment

The authors gratefully acknowledge the use of the facilities of the Center for Nanotechnology in Drug Delivery at Shiraz University of Medical Sciences (SUMS).

**Conflict of Interest:** None declared.

## References

- 1 Yan B, Gu Y, Zhao J, Liu Y, Wang L, Wang Y. Self-microemulsion Technology for Water-insoluble Drug Delivery. *Current Nanoscience*. 2019;15:576-88. doi: 10.2174/1573413715666190112122107.
- 2 Haque ST, Chowdhury EH. Recent Progress in Delivery of Therapeutic and Imaging Agents Utilizing Organic-Inorganic Hybrid Nanoparticles. *Curr Drug Deliv*. 2018;15:485-96. doi: 10.2174/1567201814666171120114034. PubMed PMID: 29165073.
- 3 Kao K-C, Mou C-Y. Pore-expanded mesoporous silica nanoparticles with alkanes/ethanol as pore expanding agent. *Microporous and mesoporous materials*. 2013;169:7-15. doi: 10.1016/j.micromeso.2012.09.030.
- 4 Nandiyanto ABD, Kim S-G, Iskandar F, Okuyama K. Synthesis of spherical mesoporous silica nanoparticles with nanometer-size controllable pores and outer diameters. *Microporous and Mesoporous Materials*. 2009;120:447-53. doi: 10.1016/j.micromeso.2008.12.019.
- 5 Vangijzegem T, Stanicki D, Laurent S. Magnetic iron oxide nanoparticles for drug delivery: applications and characteristics. *Expert Opin Drug Deliv*. 2019;16:69-78. doi: 10.1080/17425247.2019.1554647. PubMed PMID: 30496697.
- 6 Lupa D, Oćwieja M, Piergies N, Baliś A, Paluszkiwicz C, Adamczyk Z. Gold nanoparticles deposited on silica microparticles-Electrokinetic characteristics and application in SERS. *Colloid and Interface Science Communications*. 2019;33:100219. doi: 10.1016/j.colcom.2019.100219.
- 7 ALOthman ZA. A review: fundamental aspects of silicate mesoporous materials. *Materials*. 2012;5:2874-902. doi: 10.3390/ma5122874.
- 8 Gun'ko VM, Turov VV, Protsak I, Krupskaya TV, Pakhlov EM, Zhang D. Interfacial phenomena in composites with nanostructured succinic acid bound to hydrophilic and hydrophobic nanosilicas. *Colloid and Interface Science Communications*. 2020;35:100251. doi: 10.1016/j.colcom.2020.100251.

- 9 Farjadian F, Roointan A, Mohammadi-Samani S, Hosseini M. Mesoporous silica nanoparticles: synthesis, pharmaceutical applications, biodistribution, and biosafety assessment. *Chemical Engineering Journal*. 2019;359:684-705. doi: 10.1016/j.cej.2018.11.156.
- 10 Yang P, Gai S, Lin J. Functionalized mesoporous silica materials for controlled drug delivery. *Chem Soc Rev*. 2012;41:3679-98. doi: 10.1039/c2cs15308d. PubMed PMID: 22441299.
- 11 Shen SC, Ng WK, Chia L, Hu J, Tan RB. Physical state and dissolution of ibuprofen formulated by co-spray drying with mesoporous silica: effect of pore and particle size. *Int J Pharm*. 2011;410:188-95. doi: 10.1016/j.ijpharm.2011.03.018. PubMed PMID: 21419202.
- 12 Chen JF, Ding HM, Wang JX, Shao L. Preparation and characterization of porous hollow silica nanoparticles for drug delivery application. *Biomaterials*. 2004;25:723-7. doi: 10.1016/s0142-9612(03)00566-0. PubMed PMID: 14607511.
- 13 Kilpelainen M, Riikonen J, Vlasova MA, Huotari A, Lehto VP, Salonen J, et al. In vivo delivery of a peptide, ghrelin antagonist, with mesoporous silicon microparticles. *J Control Release*. 2009;137:166-70. doi: 10.1016/j.jconrel.2009.03.017. PubMed PMID: 19345247.
- 14 von Schonfeld J, Weisbrod B, Muller MK. Silibinin, a plant extract with antioxidant and membrane stabilizing properties, protects exocrine pancreas from cyclosporin A toxicity. *Cell Mol Life Sci*. 1997;53:917-20. doi: 10.1007/s000180050111. PubMed PMID: 9447243.
- 15 Romanucci V, Gravante R, Cimafonte M, Marino CD, Mailhot G, Brigante M, et al. Phosphate-Linked Silibinin Dimers (PLSd): New Promising Modified Metabolites. *Molecules*. 2017;22. doi: 10.3390/molecules22081323. PubMed PMID: 28800072; PubMed Central PMCID: PMC6152259.
- 16 Javed S, Kohli K, Ali M. Reassessing bio-availability of silymarin. *Altern Med Rev*. 2011;16:239-49. PubMed PMID: 21951025.
- 17 Patel A, Heussen P, Hazekamp J, Velikov KP. Stabilisation and controlled release of silibinin from pH responsive shellac colloidal particles. *Soft Matter*. 2011;7:8549-55. doi: 10.1039/c1sm05853c.
- 18 Cao X, Deng W, Fu M, Zhu Y, Liu H, Wang L, et al. Seventy-two-hour release formulation of the poorly soluble drug silybin based on porous silica nanoparticles: in vitro release kinetics and in vitro/in vivo correlations in beagle dogs. *Eur J Pharm Sci*. 2013;48:64-71. doi: 10.1016/j.ejps.2012.10.012. PubMed PMID: 23123331.
- 19 Ahmadi Nasab N, Hassani Kumleh H, Beygzadeh M, Teimourian S, Kazemzad M. Delivery of curcumin by a pH-responsive chitosan mesoporous silica nanoparticles for cancer treatment. *Artif Cells Nanomed Biotechnol*. 2018;46:75-81. doi: 10.1080/21691401.2017.1290648. PubMed PMID: 28278578.
- 20 Zeynizadeh B, Aminzadeh FM, Mousavi H. Green and convenient protocols for the efficient reduction of nitriles and nitro compounds to corresponding amines with NaBH<sub>4</sub> in water catalyzed by magnetically retrievable CuFe<sub>2</sub>O<sub>4</sub> nanoparticles. *Research on Chemical Intermediates*. 2019;45:3329-57. doi: 10.1007/s11164-019-03794-4.
- 21 Holzwarth U, Gibson N. The Scherrer equation versus the 'Debye-Scherrer equation'. *Nat Nanotechnol*. 2011;6:534. doi: 10.1038/nnano.2011.145. PubMed PMID: 21873991.
- 22 Cai K, He X, Song Z, Yin Q, Zhang Y, Uckun FM, et al. Dimeric drug polymeric nanoparticles with exceptionally high drug loading and quantitative loading efficiency. *J Am Chem Soc*. 2015;137:3458-61. doi: 10.1021/ja513034e. PubMed PMID: 25741752.
- 23 Ayawei N, Ebelegi AN, Wankasi D. Modeling and interpretation of adsorption isotherms. *Journal of Chemistry*. 2017;2017. doi: 10.1155/2017/3039817.
- 24 Abedi M, Abolmaali SS, Abedanzadeh M, Farjadian F, Mohammadi Samani S, Tamaddon AM. Core-Shell Imidazoline-Functionalized Mesoporous Silica Superparamagnetic Hybrid Nanoparticles as a Potential Theranostic Agent for Controlled Delivery of Platinum(II) Compound. *Int J Nanomedicine*. 2020;15:2617-31. doi: 10.2147/IJN.S245135. PubMed PMID: 32368044; PubMed Central PMCID: PMC67182466.
- 25 Borandeh S, Abdolmaleki A, Abolmaali SS, Tamaddon AM. Synthesis, structural and in-vitro characterization of beta-cyclodextrin grafted L-phenylalanine functionalized graphene oxide nanocomposite: A versatile nanocarrier for pH-sensitive doxorubicin delivery. *Carbohydr Polym*. 2018;201:151-61. doi: 10.1016/j.carbpol.2018.08.064. PubMed PMID: 30241806.
- 26 Rezaei-Sadabady R, Eidi A, Zarghami N, Barzegar A. Intracellular ROS protection efficiency and free radical-scavenging activity of quercetin and quercetin-encapsulated liposomes. *Artif Cells*



- Nanomed Biotechnol. 2016;44:128-34. doi: 10.3109/21691401.2014.926456. PubMed PMID: 24959911.
- 27 Deng J, Cheng W, Yang G. A novel antioxidant activity index (AAU) for natural products using the DPPH assay. *Food Chemistry*. 2011;125:1430-5. doi: 10.1016/j.foodchem.2010.10.031.
  - 28 Rathouský J, Schulz-Ekloff G, Had J, Zukal A. Time-resolved in situ X-ray diffraction study of MCM-41 structure formation from a homogeneous environment. *Physical Chemistry Chemical Physics*. 1999;1:3053-7. doi: 10.1039/a901968e.
  - 29 Abedi M, Abolmaali SS, Abedanzadeh M, Borandeh S, Samani SM, Tamaddon AM. Citric acid functionalized silane coupling versus post-grafting strategy for dual pH and saline responsive delivery of cisplatin by Fe<sub>3</sub>O<sub>4</sub>/carboxyl functionalized mesoporous SiO<sub>2</sub> hybrid nanoparticles: A-synthesis, physicochemical and biological characterization. *Mater Sci Eng C Mater Biol Appl*. 2019;104:109922. doi: 10.1016/j.msec.2019.109922. PubMed PMID: 31499936.
  - 30 Chiarakorn S, Areerob T, Grisdanurak N. Influence of functional silanes on hydrophobicity of MCM-41 synthesized from rice husk. *Science and Technology of Advanced Materials*. 2007;8:110. doi: 10.1016/j.stam.2006.11.011.
  - 31 Mahmoodi M, Behzad-Behbahani A, Sharifzadeh S, Abolmaali SS, Tamaddon A. Co-condensation synthesis of well-defined mesoporous silica nanoparticles: effect of surface chemical modification on plasmid DNA condensation and transfection. *IET Nanobiotechnol*. 2017;11:995-1004. doi: 10.1049/iet-nbt.2017.0078. PubMed PMID: 29155400.
  - 32 Johansson EM, Córdoba JM, Odén M. The effects on pore size and particle morphology of heptane additions to the synthesis of mesoporous silica SBA-15. *Microporous and Mesoporous Materials*. 2010;133:66-74. doi: 10.1016/j.micromeso.2010.04.016.
  - 33 Zhang Y, Zhi Z, Jiang T, Zhang J, Wang Z, Wang S. Spherical mesoporous silica nanoparticles for loading and release of the poorly water-soluble drug telmisartan. *J Control Release*. 2010;145:257-63. doi: 10.1016/j.jconrel.2010.04.029. PubMed PMID: 20450945.
  - 34 Yang C, Zhang J, Han S, Wang X, Wang L, Yu W, et al. Compositional controls on pore-size distribution by nitrogen adsorption technique in the Lower Permian Shanxi Shales, Ordos Basin. *Journal of Natural Gas Science and Engineering*. 2016;34:1369-81. doi: 10.1016/j.jngse.2016.08.026.
  - 35 Donohue M, Aranovich G. Classification of Gibbs adsorption isotherms. *Advances in colloid and interface science*. 1998;76:137-52. doi: 10.1016/S0001-8686(98)00044-X.
  - 36 Cao X, Fu M, Wang L, Liu H, Deng W, Qu R, et al. Oral bioavailability of silymarin formulated as a novel 3-day delivery system based on porous silica nanoparticles. *Acta Biomater*. 2012;8:2104-12. doi: 10.1016/j.actbio.2012.02.011. PubMed PMID: 22343518.
  - 37 Fazio E, Scala A, Grinato S, Ridolfo A, Grassi G, Neri F. Laser light triggered smart release of silibinin from a PEGylated-PLGA gold nanocomposite. *J Mater Chem B*. 2015;3:9023-32. doi: 10.1039/c5tb01076d. PubMed PMID: 32263033.
  - 38 Onken B, Traina S. The sorption of pyrene and anthracene to humic acid-mineral complexes: Effect of fractional organic carbon content. *J Environ Qual*. 1997;26:126-32. doi: 10.2134/jeq1997.00472425002600010019x.
  - 39 Bleam W. *Soil and Environmental Chemistry*. 2nd ed. Amsterdam: Elsevier; 2017.
  - 40 Atchudan R, Perumal S, Edison TNJI, Lee YR. Highly graphitic carbon nanosheets synthesized over tailored mesoporous molecular sieves using acetylene by chemical vapor deposition method. *RSC advances*. 2015;5:93364-73. doi: 10.1039/C5RA15288G.
  - 41 Carriazo D, del Arco M, Fernandez A, Martin C, Rives V. Inclusion and release of fenbufen in mesoporous silica. *J Pharm Sci*. 2010;99:3372-80. doi: 10.1002/jps.22096. PubMed PMID: 20232455.
  - 42 Sahibzada MUK, Sadiq A, Khan S, Faidah HS, Naseemullah, Khurram M, et al. Fabrication, characterization and in vitro evaluation of silibinin nanoparticles: an attempt to enhance its oral bioavailability. *Drug Des Devel Ther*. 2017;11:1453-64. doi: 10.2147/DDDT.S133806. PubMed PMID: 28553075; PubMed Central PMCID: PMC5440029.
  - 43 Lu C, Lu Y, Chen J, Zhang W, Wu W. Synchronized and sustained release of multiple components in silymarin from erodible glyceryl monostearate matrix system. *Eur J Pharm Biopharm*. 2007;66:210-9. doi: 10.1016/j.ejpb.2006.11.008. PubMed PMID: 17196805.
  - 44 Dash S, Murthy PN, Nath L, Chowdhury P. Kinetic modeling on drug release from controlled drug delivery systems. *Acta Pol Pharm*. 2010;67:217-23. PubMed PMID: 20524422.
  - 45 Singhvi G, Singh M. Review: in-vitro drug release characterization models. *Int J Pharm Stud Res*. 2011;2:77-84.